The role of direct photolysis and indirect photochemistry in the environmental fate of ethylhexyl methoxy cinnamate (EHMC) in surface water.

UNIVERSITÀ DEGLI STUDI DI TORINO

The role of direct photolysis and indirect photochemistry in the environmental fate of ethylhexyl methoxy cinnamate (EHMC) in surface waters

D. Vione[1], P. Calza[1]*, F. Galli[1], D. Fabbri[1], V. Santoro[2], C. Medana[2]

[1]*Department of Chemistry, University of Torino, via P. Giuria 5, 10125 Torino, Italy*

[2]*Department of Molecular Biotechnology and Health Sciences, University of Torino, via P. Giuria 5, 10125 Torino, Italy*

*corresponding author: e-mail: paola.calza@unito.it

Abstract

The aquatic environmental fate of ethylhexyl methoxy cinnamate (EHMC), one of the most used UVB filters worldwide, was studied by assessing its environmental persistence and photoinduced transformations. The role of direct and indirect photolysis was evaluated. Direct photolysis was shown to play a key role, and this process is expected to be the main attenuation route of EHMC in sunlit surface waters. In contrast, the reaction with •OH radicals would be negligible and that with ^{3}CDOM* would at most be a secondary process.

The measurement of the quantum yield of direct photolysis and of the rate constants of reaction with photogenerated transient species (or, sometimes, the use of reasonable values for the latter) allowed the prediction of the EHMC half-life time in surface waters, by means of a validated photochemical model. The predicted EHMC lifetime is of the order of hours to a few days in fair-weather summertime, and the main factors controlling the EHMC phototransformation in sunlit surface waters would be the water depth and the dissolved organic carbon (DOC) content.

The formation of transformation products (TPs) was followed as well *via* HPLC/HRMS. Three TPs were detected in the samples exposed to UVA radiation, while one additional TP was detected in the samples exposed to UVB radiation. The detected TPs comprised 4-methoxybenzaldehyde, a hydroxylated derivative and dimeric species. Through the use of heterogeneous photocatalysis with TiO_2, seven additional TPs were identified, most of them resulting from the further degradation of primary TPs formed through direct photolysis and that might be detected in aquatic systems as well. The photodegradation of EHMC in the presence of TiO_2 yielded more toxic TPs than the parent compound (as determined with the *Vibrio fischeri* Microtox assay). The increased toxicity is partially accounted for by the formation of 4-methoxybenzaldehyde.

Keywords: ethylhexyl methoxy cinnamate, sunscreen, photolysis, transformation products

1. Introduction

Organic UV filters are considered as pseudo-persistent environmental contaminants, although at present little is known about their distribution and impact on aquatic systems. Despite the fact that most of them are characterized by a high lipophilicity ($logK_{OW} > 3$), they can be washed away by water, thus ending up in the environment. Therefore, several sunscreens have been detected at ppb or ppt levels in surface water (Poiger et al. 2004, Rodil and Moeder, 2008,) and wastewater (Kupper et al. 2006, Magi et al. 2013), with maximum concentrations in summertime. Their hydrophobicity could also lead to accumulation in biota or sediments. Several studies have actually shown the occurrence of UV filters in aquatic organisms: the 4-methyl-benzylidene-camphor has been detected in the muscle tissue of trout in Swiss and German waters (Balmer et al. 2005), while traces of ethylhexyl methoxy cinnamate and octocrylene have been found in shellfish in the Mediterranean and Atlantic coasts of France (Bachelot et al. 2012). Furthermore, eighteen organic sunscreens were found in sediments of Japanese rivers and lakes, at concentrations ranging from 2 to about 3000 ng/g (Kameda et al. 2011). The accumulation of organic UV filters in living organisms is of major concern because some of them (and their metabolites) can act as endocrine disruptors both *in vitro* and *in vivo* (Schlumpf et al. 2001).

The present study was focused on ethylhexyl methoxy cinnamate (EHMC), also known as Eusolex 2292 and Uvinul MC80. It is one of the most used UVB filters worldwide, and it is included in the so-called High Production Volume Chemicals (HPVC) list that includes chemicals produced or imported in the EU at a rate of more than 1,000 tons per year. Although EHMC is well tolerated by the skin, it has some side effects including its ability to produce reactive oxygen species (ROS) and to penetrate in the human skin after exposure to UV light (Hanson et al. 2006, Janjua et al. 2008). The occurrence of EHMC in the environment has already been reported in many aqueous, solid and biological samples (Bachelot et al. 2012, Balmer et al. 2005, Goksoyr et al. 2009, Kameda et al. 2011, Kupper et al. 2006, Magi et al. 2013, Poiger et al. 2004, Rodil and Moeder, 2008,). EHMC has also been found in shellfish, fish and cormorants at ng/g levels, which suggests that it can be accumulated in the food chain (Fent et al. 2010). EHMC has also proved responsible for coral bleaching by promoting viral infections (Danovaro et al. 2008).

From the toxicological point of view, EHMC has estrogenic properties both *in vitro* and *in vivo* (Schlumpf et al. 2001). For instance, exposure to this compound caused the increase of the weight of the uterus in rats. Prenatal exposure to EHMC can affect both the reproductive and neurological development in the offspring of rats, which can be a cause for concern because humans are

routinely exposed to this compound through the use of sunscreens and other cosmetics (Axelstad et al. 2011).

The widespread environmental occurrence of EHMC and its negative health effects account for the importance of assessing its environmental persistence and transformation. The present work focuses on photochemical processes, which are an important class of abiotic transformation reactions that involve xenobiotics in surface waters. Previous works have studied the photostability of EHMC under cosmetic conditions (trying to simulate the behavior of the compound in solar lotions), at relatively high concentrations and without any attempt to assess or extrapolate EHMC photochemistry to sunlit surface waters (Hauri et al., 2004; Carlotti et al., 2005; Carlotti et al., 2007). The latter issue is accounted for by the fact that the previously studied systems, conditions and additives were representative of cosmetic sunscreens instead of the natural environment. Moreover, the photogenerated TPs were either not identified, or they were not tested for health or environmental effects. Therefore, previous studies do not allow an assessment of the environmental significance of EHMC phototransformation in aqueous media. The present paper has the goal of filling in the above-mentioned knowledge gaps.

Photochemical reactions in surface waters can be divided into direct photolysis and indirect photochemistry. In the case of direct photolysis, sunlight absorption by the pollutant triggers its transformation. As far as indirect photochemistry is concerned, sunlight is absorbed by photoactive compounds called photosensitisers, such as chromophoric dissolved organic matter (CDOM), nitrate and nitrite. Upon sunlight absorption, these compounds produce reactive transients such as the hydroxyl radical ($^{\bullet}OH$), singlet oxygen ($^1O_2$) and CDOM triplet states ($^3CDOM^*$), which can induce pollutant transformation (Vione et al. 2014). The role of direct photolysis and indirect photochemistry in the environmental fate of EHMC in surface waters was thus assessed, as well the phototransformation half-life time under summertime irradiation conditions that are most significant for the environmental occurrence of the studied UV filter. The TPs of EHMC were studied as well. In particular, in addition to identifying the compounds formed upon direct photolysis of the substrate, the environmental photodegradation was also simulated by the use of heterogeneous photocatalysis with titanium dioxide (TiO_2). The latter approach allows the generation of TPs that are similar to those formed by photochemical processes in the environment, as documented in several studies (Calza et al. 2010, Konstantinou et al. 2001, Calza, et al. 2011, Kouloumbos et al. 2003), and it is particularly suitable for TPs identification.

2. Experimental section

2.1. Materials

TiO_2 P25 was used as photocatalyst, after being subjected to irradiation and washings with ultrapure water in order to eliminate the potential interference caused by adsorbed ions such as chloride, sulfate and sodium. EHMC (CAS 5466-77-3, 98%), methanol (≥99.9%), acetonitrile (≥99.9%), formic acid (99%) and acetaminophen (also known as acetyl-para-aminophenol, APAP, ≥ 99.0%) were purchased from Sigma Aldrich, Italy. Rose Bengal was purchased from Alfa Aesar, Italy.

2.2. Irradiation procedures

2.2.1. Direct photolysis

Due to the low water solubility of EHMC, its aqueous solutions were prepared by methanol spiking (Rodil et al. 2009): in the case of the studies aimed at intermediate identification, solutions were prepared by adding 0.4 mL of a concentrated methanol solution of EHMC (1000 mg/L or 3.6 mM) to ultra-pure water, to obtain a final EHMC concentration of 4 mg/L (14 µM). To determine the direct photolysis quantum yield of EHMC, the used initial concentration was slightly lower (10 µM). In alternative and in comparison with methanol spiking, tests were carried out with acetonitrile spiking: fully comparable results as for methanol were obtained.

Five milliliters of aqueous solutions prepared as described above were introduced into cells of Pyrex glass (cylindrical, 4.0 cm diameter, 2.3 cm height) and subjected to irradiation. Two different lamps were used, namely a 40 W Philips TLK 05 lamp with maximum emission at 365 nm and a 20 W Philips TL 01 RS lamp with emission maximum at 313 nm. The latter lamp was also used to measure the quantum yield of EHMC direct photolysis. Due to its limited water solubility EHMC has the tendency to adsorb on the cell walls and, for this reason, the irradiated solutions were recovered from the cells by adding 5 mL of methanol that achieves desorption from the glass walls (Li et al. 2007) and allows a nearly quantitative recovery.

Figure 1 reports the absorption spectrum of EHMC, measured with a Varian Cary 100 Scan double-beam UV-vis spectrophotometer, equipped with quartz cuvettes (Hellma, 1.000 cm optical path length), as well as the emission spectrum of the TL 01 RS lamp (spectral photon flux density $p°(\lambda)$), taken with a CCD spectrophotometer (Ocean Optics USB 2000, calibrated with a DH-2000-CAL radiation source). The lamp spectrum was normalized to the results of chemical actinometry with 4-nitrobenzaldehyde. The followed procedure is described in detail by Marchisio et al. (2015).

2.2.2. Indirect photolysis

The above-described technique of methanol spiking was used in the case of indirect photolysis as well. To determine the reaction rate constants of EHMC with •OH, $^1O_2$ and CDOM triplet states, acetaminophen (APAP) was used as model compound because its reaction rate constants with the above transients are known (De Laurentiis et al. 2014). In this case, solutions containing EHMC and APAP at equal initial concentration (10 µM for both) were irradiated under suitable conditions (*vide infra*) to produce the transient species X (•OH, $^1O_2$ or ^{3}CDOM*). The time evolution of the two substrates was monitored, and the concentration *vs*. time data were fitted with the equation $C_t = C_o\, e^{-kt}$, where C_t is the substrate concentration at time *t*, C_o the initial concentration and *k* the pseudo-first order degradation rate constant. The initial transformation rate is $R = k\, C_o$. The reported error on the rates ($\pm\sigma$) mainly depended on the uncertainty on *k,* which represents the average of replicate runs.

If the degradation of the two substrates is mainly or exclusively accounted for by reaction with X, the ratio of the initial transformation rates of the two compounds can be expressed as follows:

$$\frac{R_{EHMC}}{R_{APAP}} = \frac{k_{EHMC,X}\,[X][EHMC]}{k_{APAP,X}\,[X][APAP]} = \frac{k_{EHMC,X}}{k_{APAP,X}} \qquad (1)$$

where $k_{EHMC,X}$ and $k_{APAP,X}$ are the second-order reaction rate constants with X of EHMC and APAP, respectively, [X] is the steady-state concentration of the transient (note that EHMC and APAP are in the same solution) and [EHMC] = [APAP] = 10 µM are the initial concentration values of the two substrates. The equation can be simplified and one gets that the ratio of the initial rates is equal to the ratio of the second-order rate constants. Therefore, by knowing the rate constant $k_{APAP,X}$ (De Laurentiis et al. 2014) and by measuring the initial degradation rates, one gets $k_{EHMC,X} = k_{APAP,X}\, R_{EHMC}\,(R_{APAP})^{-1}$.

The radical •OH was produced by irradiating 1 mM H_2O_2 under the TLK 05 or the TL 01 RS lamp, while anthraquinone-2-sulfonate (AQ2S) was used as CDOM proxy to study the reactivity of ^{3}CDOM* (De Laurentiis et al. 2014). In this case, 1 mM AQ2S was irradiated under the TLK 05 lamp. Measures of reactivity with $^1O_2$ were performed using a lamp Philips TL D 18W/16 with emission maximum at 545 nm. The dye Rose Bengal (10 µM initial concentration) was chosen as the source of singlet oxygen. Also in the indirect photolysis experiments, at the end of the irradiation, the content of the cells was recovered with 5 mL of methanol. In all the cases, the pH of the irradiated solutions was 6-6.5.

2.2.3. Photocatalysis

The irradiation with TiO_2 of a compound that is poorly water-soluble can be carried out by dispersing in water the photocatalyst loaded with the substrate. To do so, a EHMC stock solution was prepared in methanol at the concentration of 15 mg/L. The photocatalyst powder was added to obtain a TiO_2 loading of 200 mg/L, then the solvent was evaporated with a Büchi Rotavapor system so as to obtain a TiO_2 powder loaded with EHMC. The latter was suspended in water, at a loading that depended on the type of experiment.

Five milliliters of the suspension thus obtained were introduced into the Pyrex cells and irradiated under the Philips TLK 05 lamp. After irradiation the content of the cells was recovered with 5 mL methanol to prevent EHMC loss upon adsorption on the glass, and the slurry was filtered on a 0.45 µM filter (PTFE, Merck Millipore, Milan, Italy).

2.3. Analytical techniques

2.3.1. HPLC-UV

A VWR-Hitachi LaChrom Elite chromatograph, equipped with a L-2300 autosampler (injection volume 60 µL), a quaternary pump module L-2130, a L-2300 column oven (temperature 40 °C), a DAD detector L-2445, and a reverse-phase column (VWR RP-C18 LiChroCART, 4 mm × 125 mm × 5 µm) was used to measure the direct photolysis quantum yield of EHMC and its reaction rate constants with the transient species. To determine both EHMC and APAP, a gradient of methanol and phosphoric acid (3 mM) with 1 mL/min flow rate, by increasing the methanol percentage from 15 to 90% in 15 min, was used.

In other experiments, EHMC was monitored by using a Merck-Hitachi chromatograph equipped with a Rheodyne injector, L-6200 and L-6200A pumps for high-pressure gradients, a L-4200 UV-Vis detector, and the same column as above. Isocratic elution (1 mL/min flow rate) was carried out with 20% of 10 mM phosphate buffer (H_3PO_4 + NaH_2PO_4) at pH 2.8 and 80% acetonitrile. The retention time of EHMC was 7.4 min and the detection wavelength was set at 310 nm.

2.3.2. HPLC-HRMS

The chromatographic separations, monitored using an MS analyzer, were run on a Phenomenex Luna C18 (2) 150 × 2.1 mm × 3 µm particle size, using an Ultimate 3000 HPLC instrument (Dionex, Thermo Scientific, Milan, Italy). The injection volume was 20 µL and the flow rate 200 µL/min. Gradient mobile phase composition was adopted: A/B was varied from 5/95 to 100/0 in 35

min (followed by 10 minutes of 100% A isocratic elution), where A = acetonitrile and B = formic acid 0.05 % v/v in water, when run on ESI positive ion mode.

A LTQ Orbitrap mass spectrometer (Thermo Scientific, Milan, Italy) equipped with an ESI ion source was used. The LC column effluent was delivered into the ion source using nitrogen as both sheath and auxiliary gas. The tuning parameters adopted for the ESI source were: capillary voltage 37.00 V, tube lens 65 V. The source voltage was set to 3.5 kV. The heated capillary temperature was maintained at 275°C. The acquisition method used was optimized before and in the tuning sections for the parent compound (capillary, magnetic lenses and collimating octapole voltages) to achieve maximum sensitivity. Mass accuracy of recorded ions (vs. calculated) was ± 10 millimass units (mmu) without internal calibration. External calibration was performed with a mixture of caffeine, MRFA peptide and Ultramark 1621 (LTQ calibration solution, Thermo Scientific, Milan, Italy).

Analyses were run using full MS (50-1000 *m/z* range), MS^2 and MS^3 acquisition in the positive ion mode, with a resolution of 30000 (500 *m/*z FWHM) in FTMS mode. The ions submitted to MS^n acquisition were chosen on the base of full MS spectra abundance without using automatic dependendent scan. Collision energy was set to 30 (arbitrary units) for all of the MS^n acquisition methods. MS^n acquisition range was between the values of ion trap cut-off and *m/z* of the fragmented ion. Xcalibur 2.0.7 (Thermo Scientific, Milan, Italy) software was used both for acquisition and for elaboration.

2.4. Photochemical modeling

The assessment of the phototransformation kinetics was carried out with the APEX software (Aqueous Photochemistry of Environmentally-occurring Xenobiotics). It predicts photochemical half-life times as a function of water chemistry and depth, for compounds with known direct photolysis quantum yields and second-order reaction rate constants with transient species. APEX is based on a photochemical model, validated by comparison with field data of phototransformation kinetics in surface freshwaters (Maddigapu et al., 2011; Vione et al., 2011; De Laurentiis et al., 2012; Marchetti et al., 2013; Bodrato and Vione, 2014). The previous validation of the model against available field data of several pollutants justifies the use of APEX also in the present case, where data of EHMC phototransformation in surface waters are unfortunately unavailable.

APEX results apply to well-mixed water bodies, including the epilimnion of stratified lakes. The absorption of radiation by photosensitisers (CDOM, nitrate and nitrite) and xenobiotics is computed by taking into account competition for sunlight irradiance in a Lambert-Beer approach.

Data obtained with APEX are averages over the water column of given depth, and they include the contributions of the well-illuminated surface layer and of darker water at the bottom.

Sunlight irradiance is not constant in the natural environment, because of meteorological issues (not included in APEX) and of diurnal and seasonal cycles. To allow easier comparison between model results and environmental conditions, APEX uses as time unit a summer sunny day (SSD), equivalent to fair-weather 15 July at 45° N latitude. Another issue is that sunlight is not vertically incident over the water surface, but refraction at the interface deviates the light path in water towards the vertical. The light path length l depends on the depth d: on 15 July at 45°N it is $l = 1.05\ d$ at noon and $l = 1.17\ d$ at ±3 h from noon, which is a reasonable daily average (Bodrato and Vione, 2014).

2.5. Prediction of toxicity towards freshwater organisms

Insight into the possible acute and chronic toxicity of the TPS of EHMC was obtained by ECOSAR software (Ecological Structure Activity Relationship, *http://www.epa.gov/oppt/newchems/tools/21ecosar.htm*, last accessed April 2015), which gives a standard toxicity profile based on calculated acute and chronic effects on fish, daphnia and algae. Calculations are carried out with a quantitative structure-activity relationship approach, based on class-specific linear regressions (Tunkel et al. 2005).

2.6. Toxicity Measurements (Microtox)

The toxicity of samples collected at different irradiation times was evaluated with a Microtox Model 500 Toxicity Analyzer (Milan, Italy). Acute toxicity was evaluated with a bioluminescence inhibition assay using the marine bacterium *Vibrio fischeri*, by monitoring changes in the natural emission of the luminescent bacteria when challenged with toxic compounds. Freeze-dried bacteria, reconstitution solution, diluent (2% NaCl) and an adjustment solution (non-toxic 22% sodium chloride) were obtained from Azur (Milan, Italy). Samples were tested in a medium containing 2% sodium chloride, in five dilutions, and luminescence was recorded after 5, 15 and 30 min of incubation at 15^{o} C. Because no substantial differences were found between the three contact times, hereafter the results related to 5 minutes of contact are reported. Inhibition of luminescence, compared with a toxic-free control to give the percentage inhibition, was calculated following the established protocol and using the Microtox calculation program.

3. Results and discussion

3.1. Assessment of EHMC phototransformation in surface waters

When irradiated alone under the TL 01 RS lamp under ~neutral pH conditions, 10 µM EHMC showed an initial degradation rate R_{EHMC} = (1.72±0.15)·10^{-9} M s^{-1}. The photon flux absorbed by EHMC is $P_a^{EHMC} = \int_\lambda p°(\lambda)[1-10^{-\varepsilon_{EHMC}(\lambda)b[EHMC]}]d\lambda$ = 4.5·10^{-8} Einstein L^{-1} s^{-1}, where $p°(\lambda)$ and $\varepsilon_{EHMC}(\lambda)$ are reported in Figure 1, b = 0.4 cm and [EHMC] = 1.0·10^{-5} M. The photolysis quantum yield can be calculated as $\Phi_{EHMC} = R_{EHMC}(P_a^{EHMC})^{-1}$ = (3.8±0.3)·10^{-2}. Because the used lamp shows an emission maximum that is close to the absorption maximum of EHMC and because the relevant band is also responsible for sunlight absorption by EHMC, the calculated photolysis quantum yield is representative of EHMC photodegradation under sunlight (Turro et al. 1978).

The reaction rate constant between EHMC and $^1O_2$ was measured by irradiating 10 µM of EHMC and 10 µM of APAP under the TL D 18W/16 lamp, in the presence of 10 µM Rose Bengal as $^1O_2$ source. Under the reported conditions it was R_{EHMC} = (5.26±0.85)·10^{-11} M s^{-1} and R_{APAP} = (1.26±0.27)·10^{-10} M s^{-1}. Considering that the second-order reaction rate constant $k_{APAP,^1O_2}$ = (3.68±0.73)·10^7 M^{-1} s^{-1} (De Laurentiis et al. 2014), one gets $k_{EHMC,^1O_2} = k_{APAP,^1O_2} R_{EHMC}(R_{APAP})^{-1}$ = (1.54±0.88)·10^7 M^{-1} s^{-1}.

Unfortunately it was not possible to measure the reaction rate constants of EHMC with $^\bullet$OH and ^{3}AQ2S* (taken as representative of ^{3}CDOM*), because irradiation under UVB and UVA caused an important direct photolysis of EHMC. Under such circumstances, the prerequisites behind equation (1) are not valid and the reaction rate constants cannot be measured. In the case of $^1O_2$, the measurement was allowed by the fact that the used lamp emits yellow light that is not absorbed by EHMC. Anyway, possible values of the rate constants with $^\bullet$OH and ^{3}CDOM* were considered in photochemical modeling. Moreover, the important interference of direct photolysis in the above irradiation experiments suggests that the direct photoprocess could also play a key role in the environmental transformation of EHMC.

Figure 2a reports the modeled half-life time of EHMC (in SSD units, namely summer sunny days equivalent to 15 July at 45°N latitude) as a function of water depth and of the dissolved organic carbon (DOC). The relevant calculations considered only the direct photolysis and the reaction with $^1O_2$, thus the results are actually upper limits for the EHMC lifetimes. Despite this, it

can be noticed that the phototransformation would be very fast because $t_{½}$ < 1.5 SSD even in relatively deep water with high DOC concentration. Also note that reaction with $^1O_2$ would play a negligible role compared to the direct photolysis, thus the reported results almost exclusively depend on the direct phototransformation.

The figure shows that the half-life time increases with increasing depth and DOC. The trend with depth is accounted for by the fact that the bottom layers of deep water bodies are poorly illuminated by sunlight and, therefore, they are poorly photoactive. In deep waters, the high photoactivity of the surface layer is offset by the poor reactivity in the lower depths. As far as the trend with DOC is concerned, high-DOC waters usually contain abundant CDOM that competes with the pollutants for sunlight irradiance, thereby inhibiting the direct photolysis processes (Vione et al. 2014).

As mentioned above, the reaction rate constants of EHMC with $^{\bullet}$OH and ^{3}CDOM* are unfortunately not available. However, bimolecular reaction rate constants in aqueous solution have the diffusion control as an upper limit (Buxton et al. 1988). For this reason, the expected importance of the different phototransformation pathways was also assessed by assuming that $k_{EHMC,^{\bullet}OH}$ could vary up to $2 \cdot 10^{10}$ M^{-1} s^{-1} and $k_{EHMC,^3CDOM*}$ up to $1 \cdot 10^{10}$ M^{-1} s^{-1}. The difference between the two values is due to the fact that $^{\bullet}$OH is generally more reactive than ^{3}CDOM* (Vione et al. 2014). With these assumptions it can be concluded that, under the surface-water conditions reported in Figure 2a, $^{\bullet}$OH would never account for more than 1% of EHMC phototransformation and the relative role of ^{3}CDOM* would always be below 10%. As a consequence, the EHMC photodegradation would mainly take place upon direct photolysis, while the reaction with $^{\bullet}$OH would be negligible and that with ^{3}CDOM* would at most be a secondary process. The concentrations of nitrate, nitrite, carbonate and bicarbonate in water mainly affect the $^{\bullet}$OH reaction (Vione et al. 2014), thus the relevant concentration variations would not modify significantly the modeled half-life time of EHMC. In summary, the main factors controlling the phototransformation of this compound in surface waters would be the water depth and the DOC.

Because the direct photolysis is expected to be the main EHMC phototransformation pathway in surface waters, it is important to identify the TPs that are produced during this process. Among the identified TPs (*vide infra*), 4-methoxybenzaldehyde (MOBA) was available as commercial standard. The transformation yield of EHMC into MOBA upon direct UVB photolysis was thus found to be η_{MOBA} = 1.6% (the disappearance of 13 µM EHMC yielded 0.21 µM MOBA). The yield datum allows the modeling of MOBA formation (Bodrato and Vione, 2014). Moreover, if the first-order degradation rate constant of MOBA (k_{MOBA}) were available, it would be possible to predict the time trends of both EHMC and MOBA due to photochemical reactions. Under the

pseudo-first order approximation, the time trend of EHMC would be described by $[EHMC]_t = [EHMC]_o\ e^{-k_{EHMC}\,t}$, where $[EHMC]_t$ is the concentration of EHMC at the time *t*, $[EHMC]_o$ its initial concentration and k_{EHMC} the (APEX-modeled) pseudo-first order degradation rate constant of EHMC. The time trend of MOBA (resulting from the budget of formation from EHMC and transformation) would be described by $[MOBA]_t = \eta_{MOBA}\ k_{EHMC}\ [EHMC]_o\ (k_{EHMC} - k_{MOBA})^{-1}\ [\exp(-k_{MOBA}\ t) - \exp(-k_{EHMC}\ t)]$, where $[MOBA]_t$ is the concentration of MOBA at the time *t* and the other variables have been already defined (Ruggeri et al., 2014). It was also assumed $[MOBA]_o = 0$ M.

It is possible to make some assumptions on the possible value of k_{MOBA} by hypothesising that MOBA only reacts with •OH ($k°_{MOBA}$), that $k'_{MOBA} = 2\ k_{EHMC}$ (that is, MOBA is twice more photolabile than EHMC), as well as intermediate cases. With surface-water conditions that middle-way in the plot of Figure 2a (5 mg C L^{-1} DOC, 5 m depth, 0.1 mM nitrate, 1 µM nitrite, 1 mM bicarbonate and 10 µM carbonate) one gets $k_{EHMC} = 3.3\ SSD^{-1}$ and $[•OH] = 1.6 \cdot 10^{-17}$ M. With these data, by assuming that MOBA reacts with •OH with a near-diffusion second-order reaction rate constant ($2 \cdot 10^{10}\ M^{-1}\ s^{-1}$), one obtains $k°_{MOBA} = 0.01\ SSD^{-1}$ and $k'_{MOBA} = 6.6\ SSD^{-1}$. Figure 2b reports the time trends (SSD units) of the concentrations of EHMC and MOBA, referred to the above water conditions and for different values of k_{MOBA} (ranging from $k°_{MOBA}$ to k'_{MOBA}). The plot shows that $[MOBA]_t \leq 0.02\ [EHMC]_o$, which could limit the possible environmental impact of MOBA. However, this possible conclusion is strongly questioned by toxicity measurements (*vide infra*).

3.2. Identification of the TPs of EHMC upon direct photolysis

Direct photolysis experiments were performed by subjecting an aqueous solution of EHMC (4 mg L^{-1}) to UVA and UVB radiation. The UVB radiation was more effective than UVA to degrade the sunscreen, as shown by the EHMC time trend reported in Figure 3: half-life time passed from 250 min under UVA to 30 min under UVB. After 4 hours of irradiation, EHMC was almost completely degraded under UVB irradiation, while only 50% was eliminated under UVA.

3.2.1. MS^n spectra of EHMC

EHMC was detected as $[M+H]^+$ 291.1952 in ESI positive mode. The MS^n study provided useful information to identify unknown TPs formed through the degradation process. The product ions generated from the protonated molecular ions of EHMC are listed in Table S1 and a pattern of fragmentation for EHMC is shown in Scheme S1. The MS^2 spectrum shows the formation of two product ions at 179.0701 *m/z*, due to the loss of the alkyl chain, and at 161.0594 *m/z*, coming from

the combined loss of the alkyl chain and a water molecule. These routes have been carefully considered in the structure attribution of the unknown compounds presented below.

3.2.2. Transformation products

Following EHMC degradation, several TPs were identified. In samples subjected to UVB radiation, the species at *m/z* 137.0591 (named **I**), 307.1806 (**II**), 469.2589 (**III**) and 581.3851 (**IV**) were identified. In the samples subjected to UVA radiation, only the species **I**, **II** and **IV** were detected. The detected intermediates are listed in Table 1, while their evolution over time is plotted in Figure 4. In both cases, the most abundant TP was compound **I**.

HRMS analysis allowed the attribution of empirical formulas to these species, which were then characterized by MS^n spectra interpretation.

The species 137.0591 *m/z* (named **I**) was assumed to be the 4-methoxybenzaldehyde (MOBA), as already reported in the literature (Deblonde et al. 2011), which was confirmed by injection of a standard solution. The species **II** with 307.1806 *m/z* was attributed to monohydroxylated EHMC; the proposed pattern of fragmentation is shown in Scheme 1. The product ion at 195.0660 *m/z* results from the loss of an unmodified alkyl chain (C_8H_{16}), while the product ion 135.0442 *m/z* was formed through the combined loss of alkyl chain and acetic acid. Finally, 177.0551 *m/z* derives from the detachment of the alkyl chain and a molecule of water. Following the MS^n experiments, it was possible to recognize that hydroxylation involves the left side of the molecule and, in particular, we tentatively placed the hydroxyl group on the α carbon atom.

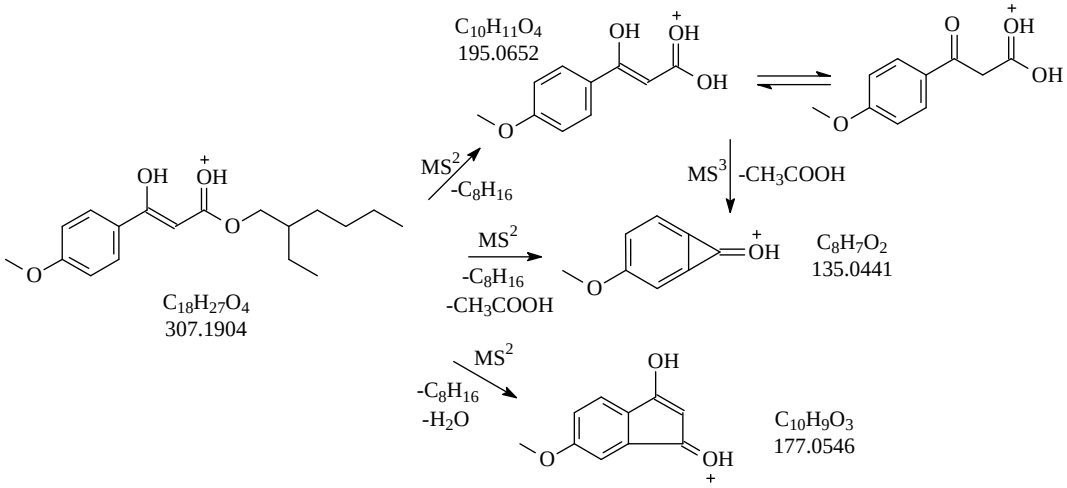

Scheme 1. Proposed fragmentation pathway for 307.1904 *m/z* (**II**)

The other two TPs, named **III** and **IV**, involved an EHMC dimerization. TP with 581.3851 *m/z* (**IV**) with empirical formula $C_{36}H_{53}O_6$ and TP with 469.2589 *m/z* (**III**) with empirical formula $C_{28}H_{37}O_6$ are well-matched with the dimerization products already documented in the literature (Rodil et al. 2009). The hypothesized fragmentation pattern for TP **III** is illustrated in Scheme 2.

Interestingly, the dimerization of EHMC under UV irradiation has been reported in several studies (see for instance Hanson et al. (in press), and references therein). Curiously, we did not detect photoisomerization of EHMC, differently from previous reports, but it should be pointed out that our irradiation experiments were carried out in water, while the photoisomerization pathway is favored in organic solvents. In contrast, the aqueous solution favors alternative pathways that have only beenmarginally characterized in previous studies (Hanson et al., in press), and that the present work helps in elucidating. Also interestingly, the photostability of EHMC in organic solvents is attributed to the short lifetime of its excited states, and particularly of the triplet one (Kikuchi et al., 2014). However, triplet states in aqueous solution could react with the solvent to produce water adducts and, finally, hydroxy derivatives. For instance, in the case of anthraquinone-2-sulphonate, the reaction of its triplet state with water is so fast as to prevent the formation of 1O2 from the triplet state itself and dissolved oxygen (Bedini et al., 2012). In the case of EHMC, the detection of several hydroxy derivatives upon direct photolysis in aqueous solution could be compatible with (although not making compelling evidence for) such a reaction with the solvent.

By applying the ECOSAR software to EHMC and to compounds **I-IV** it was possible to get some insight into the possible effects of the transformation intermediates on aquatic organisms, compared to the parent molecule (see Table S2(SM) for the detailed ECOSAR results). An interesting issue is that **I** (MOBA), the most abundant intermediate as far as peak area is concerned, is predicted to be much less toxic than EHMC considering all acute and chronic endpoints. Note, however, that ECOSAR predicts toxicity for fish, daphnid and algae. Quite different results were obtained in the case of *Vibrio fischeri* bacteria (*vide infra*). The toxicity of **II** and **III** would be comparable to that of EHMC but a bit lower (particularly in the case of **II**). The predicted LC50, EC50 and ChV values for these compounds would be in the ppb to ppm range. Finally, **IV** is predicted to be significantly more toxic than EHMC for aquatic organisms (all endpoints concerned). For both EHMC and compounds **II**-**IV**, the highest acute effects are expected for algae and the highest chronic effects for fish. In the case of **IV**, it should be considered that it is a dimeric species and that its formation from EHMC would strongly depend on the concentration of the parent compound. To allow easier identification of the intermediates, the used concentration of EHMC (4 mg/L) was considerably higher than its usual levels in surface waters (Magi et al. 2013, Poiger et al. 2004, Rodil and

Moeder, 2008), where the probability to produce **IV** through direct photolysis would be much lower than in the investigated laboratory systems.

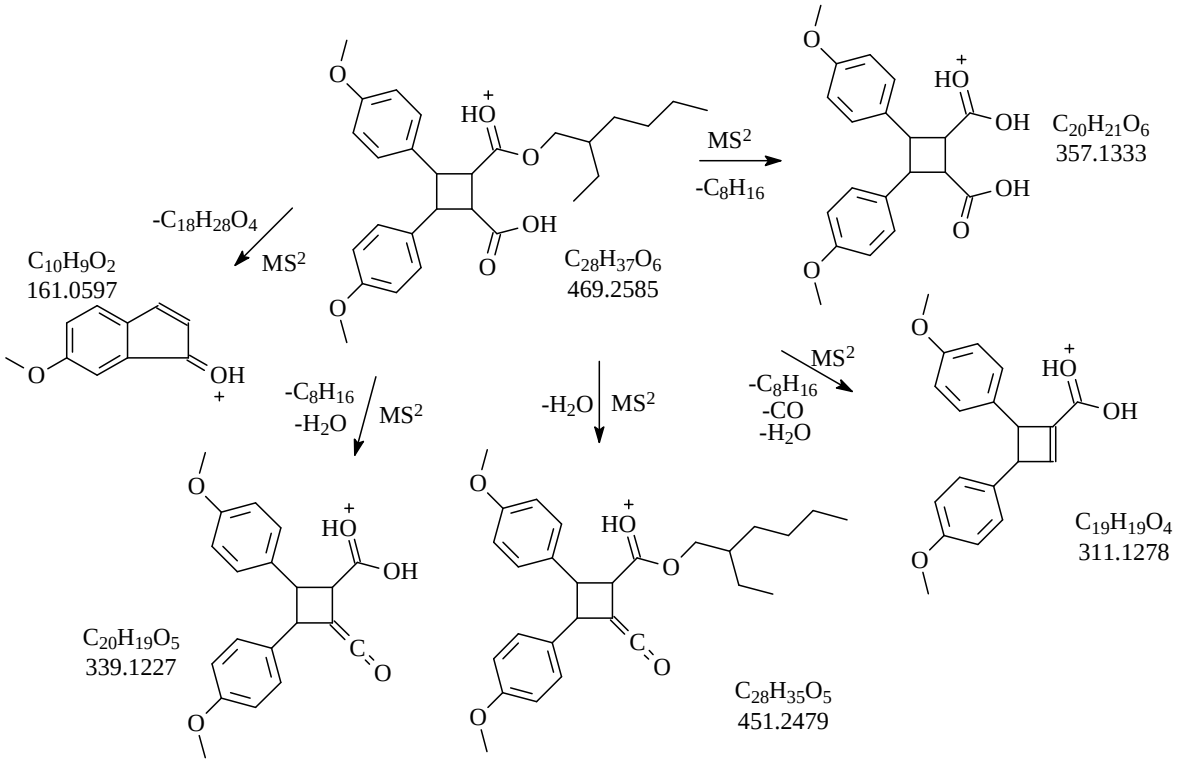

Scheme 2. Fragmentation pattern of the dimeric species 469.2589 (**III**).

3.3. Heterogeneous photocatalysis

The addition of titanium dioxide increased the degradation rate of EHMC under UVA and its half-life time was shortened to 40 min, as shown in Figure 5. Analyzing the formation of TPs, their time-trend profiles under heterogeneous photocatalysis are presented in Figure 5. Species **I** and **II,** already detected through the direct photolysis process, were formed, while **III** and **IV** were absent. **I** was the main TP, as already reported under direct photolysis. Besides, the photocatalytic process triggered new pathways and seven additional TPs were identified. The species at 179.0703 *m/z* (named **VI**) showed a maximum after four hours of irradiation, then it decreased and it was eliminated within 16 hours. MS^2 and MS^3 spectra analyses allowed its identification as 4-methoxycinnamic acid, confirmed by injection of a standard solution. Data are reported in Table S1, while the proposed fragmentation pathways are shown in Figure S1.

An additional monohydroxylated derivative was formed, named **V**. Its MS^2 spectrum presents the product ions 179.0708 and 161.0600 *m/z*. Interestingly, the same ions were formed in the MS^2

spectrum of EHMC, and they are well-matched with the loss of the alkyl chain carrying a hydroxyl group. These ions allowed to locate the hydroxyl group on the alkyl chain (see Figure S2).

Three isobaric species (named **VII-IX**), with 323.1850 *m/z* and molecular formula $C_{18}H_{27}O_5$ were found, well-suited to a double EHMC hydroxylation. The MS^2 and MS^3 spectra showed the formation of the product ions summarized in Table S1, while their patterns of fragmentation are shown below in Scheme 3. Considering isomer **A** (named **VII**), the presence of the structural-diagnostic ion at 161.0597 *m/z* in the spectrum of MS^2, resulting from the loss of the alkyl chain plus two oxygen atoms, suggests that the alkyl chain has undergone transformation.

Conversely for the isomers **B** and **C**, the formation of the product ion with 211.0610 *m/z* in the MS^2 spectrum, consistent with the loss of the unmodified alkyl chain, suggests that both hydroxylations are located on the left part of the molecule. For isomer **B** (named **VIII**), the MS^3 spectrum presents the other structural-diagnostic ion 121.0281 *m/z*, formed through a concerted loss of 2-hydroxypropenoic acid and water, which assesses the presence of an hydroxyl group on this moiety. Therefore, the occurrence of more than one hydroxylation on the aromatic ring can be excluded. For isomer **C** (named **IX**) the MS^3 spectrum presents the structural-diagnostic ion 135.0437 *m/z*, which allows the location of the two hydroxylations on the carbons in positions β to the aromatic ring. The second OH group could be located in carbon α or on the aromatic ring.

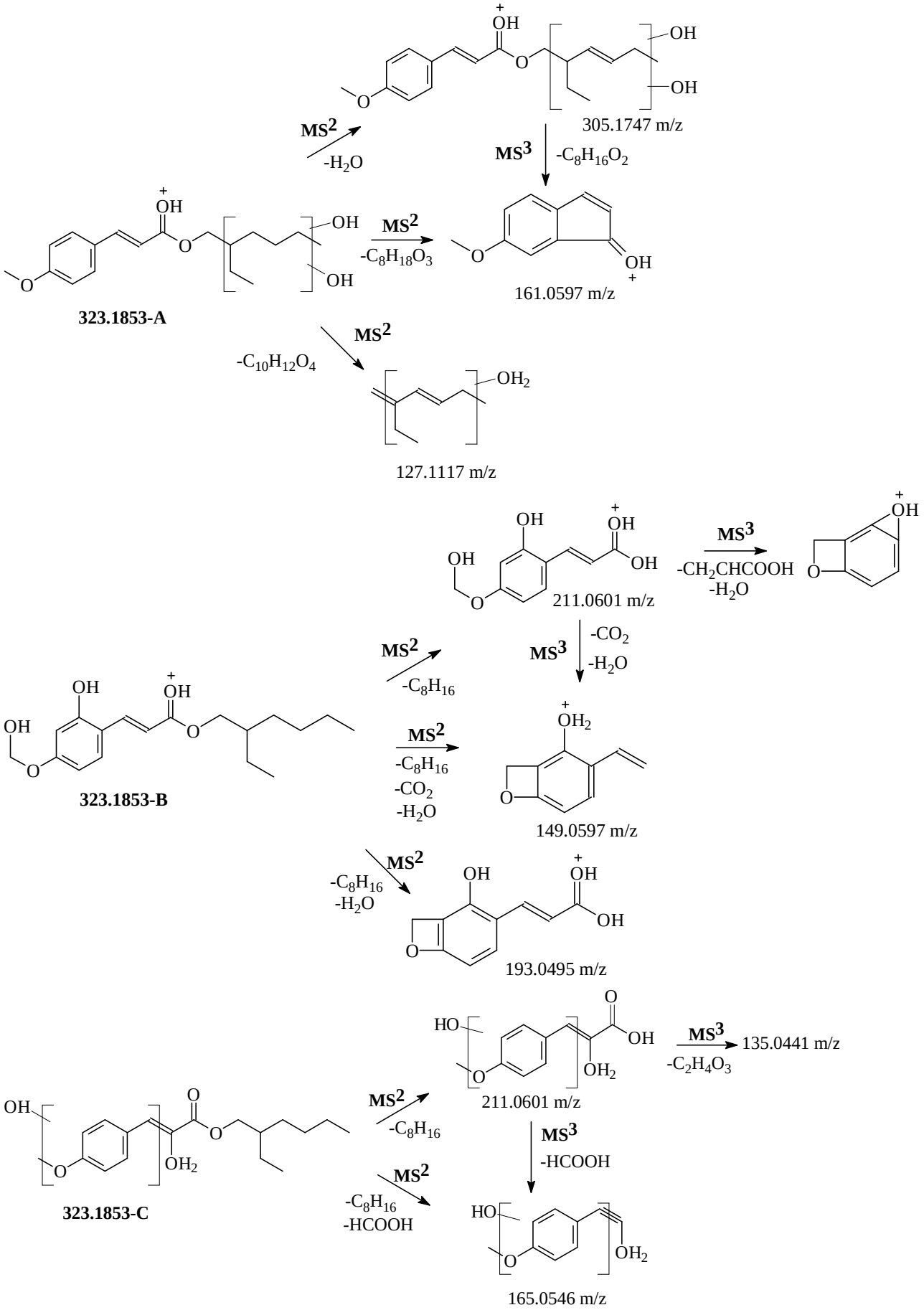
305.1747 m/z
MS2
-H2O
MS3
-C8H16O2
MS2
-C8H18O3
161.0597 m/z
323.1853-A
MS2
-C10H12O4
127.1117 m/z
211.0601 m/z
MS3
-CH2CHCOOH
-H2O
MS2
-C8H16
MS3
-CO2
-H2O
323.1853-B
MS2
-C8H16
-CO2
-H2O
149.0597 m/z
MS2
-C8H16
-H2O
193.0495 m/z
211.0601 m/z
MS3
135.0441 m/z
-C2H4O3
MS2
-C8H16
MS3
-HCOOH
323.1853-C
MS2
-C8H16
-HCOOH
165.0546 m/z

Scheme 3. Fragmentation pathways of the species with 323.1850 *m/z* (**VII**, **VIII** and **IX)**.

Two isobaric species with 305.1732 *m/z* and molecular formula $C_{18}H_{25}O_4$, labelled **X** and **XI**, were identified and attributed to monohydroxylated/oxidized derivatives. The MS^2 spectra for both isomers allowed the proposal of oxidation on the alkyl chain, due to the presence of ions 161.0601 and 179.0709 *m/z*. Unfortunately, there is not enough information to properly locate the oxidized moiety.

A definite chemical formula could thus be suggested for the intermediates **VI**, **VIII** and **IX**, and the ECOSAR software could be used to get insight into their possible acute and chronic toxicity. For all the considered endpoints, all these intermediates (and most notably **VI**) are expected to be much less toxic than the parent EHMC.

3.4. EHMC transformation pathways

All the characterized TPs resulting from EHMC photoinduced degradation could be linked together according to the pathways summarized in Figure 6.

The identified TPs could be formed following six concomitant pathways: routes **A** and **F**, involving EHMC dealkylation; paths **B** and **C**, following mono or di-hydroxylation, as well as paths **D** and **E**, involving the molecule dimerization and occurring only through direct photolysis.

Route **A**, leading to the formation of MOBA, was the main transformation pathway under both direct photolysis and heterogeneous photocatalysis. The path **B**, involving mono hydroxylation, seems to play an important role in both photolysis and photocatalysis processes, with the predominant formation of the species **II**. The formation of 4-methoxycinnamic acid *via* dealkylation (path **F**) is a favored process, too. Taking into account the temporal evolution profiles, it can be assumed that dihydroxylated species (**VII**, **VIII** and **IX**) and hydroxylated/oxidized species (**X** and **XI**) resulted from the degradation of mono-hydroxylated TPs.

3.5. Toxicity assessment

Acute toxicity was evaluated by monitoring changes in the natural emission of the luminescent bacteria *Vibrio fischeri* when challenged with toxic compounds, and it was expressed as percentage of inhibition of the bacteria luminescence. Results obtained on samples subjected to heterogeneous photocatalysis are plotted in Figure 7.

While EHMC was scarcely toxic (30% luminescence inhibition), its transformation proceeded through the formation of harmful compounds, as shown by the percentage of inhibition effect that increased as a function of the irradiation time. Indeed, acute toxicity increased up to 70-80% from 1 h onward and it remained almost stable for up to 24 h irradiation. This shape exhibits a good overlap (at least up to 8 h irradiation) with the time evolution of compound **I** (MOBA), which is more toxic than EHMC (EC_{50}= 3 mg/l) and seems to be the TP mainly responsible for the acute toxicity observed at $t_{irradiation} \leq 8$ h. This is very interesting when considering the relatively low transformation yield of EHMC into MOBA (see Figure 5).

Another issue is that, while MOBA is quite toxic to *Vibrio fischeri* bacteria, its modeled toxicity for higher organisms was pretty low. Therefore, its environmental impact might be very species-specific.

Conclusions

The results obtained suggest that the direct photolysis is the main removal route for EHMC in the aquatic environment, while the indirect photochemistry plays a negligible or minor role (degradation by ^{3}CDOM* could be somewhat important in deep and DOM-rich environments). The quantified intermediate **I** (MOBA) is formed in relatively low yield (1.6%) upon EHMC direct photolysis, but this issue does not necessarily imply a low environmental impact. The characterization of transformation products performed *via* HPLC-HRMS showed that EHMC is transformed into four TPs under UVB irradiation. Through heterogeneous photocatalysis, additional TPs were formed and identified: they may also be formed in aquatic systems.

The toxicity of the irradiated mixtures was directly measured with the Microtox assay. Moreover, by applying the ECOSAR software to EHMC and the identified TPs it was possible to get some insight into their possible effects on aquatic organisms (fish, daphnid, algae). The intermediate MOBA is more toxic than EHMC towards bacteria and it accounts for an important fraction of the measured toxicity at relatively short irradiation times, which is remarkable given its low formation yield from EHMC. However, MOBA might not be very toxic for higher organisms. The compound **IV** could be very toxic to aquatic organisms, but as a dimeric species its formation would presumably require much higher substrate concentrations than those actually found in natural surface waters.

Acknowledgements

This work has been financed through the project funded by MIUR, in the frame of the collaborative international consortium WATERJPI2013-MOTREM of the Water Challenges for a Changing World Joint Programming Initiative (WaterJPI) Pilot Call. D.V. also acknowledges financial support by Università di Torino / Compagnia di San Paolo - EU Accelerating Grants, project TO_Call2_2012_0047 (DOMNAMICS).

References

Axelstad M.; Boberg J.; Hougaard K.S.; Christiansen S.; Rosenskjold Jacobsen P.; Riiber Mandrup, K.; Nellemann C.; Lund S.P.; Hass U. Effects of pre- and postnatal exposure to the UV-filter Octyl Methoxycinnamate (OMC) on the reproductive, auditory and neurological development of rat offspring; Toxicol. Appl. Pharmacol. 2011; 250: 278–290

Bachelot M.; Li Z.; Munaron D.; Le Gall P.; Casellas C.; Fenet H.; Gomez E.; Organic UV filter concentrations in marine mussels from French coastal regions; Sci. Total Environ. 2012; 420: 273-9

Balmer M.; Buser H.R.; Müller M.D.; Poiger T.; Occurrence of Some Organic UV Filters in Wastewater, in Surface Waters, and in Fish from Swiss Lakes; Environ. Sci. Technol. 2005; 39: 953–962

Bodrato M., Vione D., APEX (Aqueous Photochemistry of Environmentally occurring Xenobiotics): A free software tool to predict the kinetics of photochemical processes in surface waters. Environ. Sci.: Processes and Impacts 2014; 16: 732-740.

Buxton G.V., Greenstock C.L., Helman W.P., Ross A.B., Critical review of rate constants for reactions of hydrated electrons, hydrogen atoms and hydroxyl radicals ($^{\bullet}OH/O^{-\bullet}$) in aqueous solution. J. Phys. Chem. Ref. Data 1988; 17: 1027-1284.

Calza P.; Medana C.; Raso E.; Gianotti V.; Minero C.; N,N-diethyl-m-toluamide transformation in river water; Sci. Tot. Environ., 2011; 409: 3894-3901

Calza P.; Marchisio S.; Medana C.; Baiocchi C.; Fate of the antibacterial spiramycin in river waters; Anal. Bioanal. Chem. 2010; 396 (4):1539-1550

Carlotti, M.E.; Sapino, S.; Vione, D.; Pelizzetti, E.; Ugazio, E.; Morel, S. Study on the photostability of octyl-p-methoxy cinnamate in SLN. J. Disp. Sci. Technol. 2005; 26: 809-816

Carlotti, M.E.; Sapino, S.; Vione, D.; Minero, C.; Trotta, M.; Gallarate, M. Photostability of octyl-p-methoxy cinnamate in O/W emulsions and in SLNs vehicled in the emulsions. J. Disp. Sci. Technol. 2007; 28: 1034-1043

Danovaro R.; Bongiorni L.; Corinaldesi C.; Giovannelli D.; Damiani E.; Astolfi P.; Sunscreens cause coral bleaching by promoting viral infections; Environ. Health Perspect. 2008; 116:441–7

Deblonde T.; Cossu-Leguille C.; Hartemann P.; Emerging pollutants in wastewater: A review of the literature; Internat. J. Hygiene Environ. Health 2011; 214 (6) 442-448

De Laurentiis E., Chiron S., Kouras-Hadef S., Richard C., Minella M., Maurino V., Minero C., Vione D. Photochemical fate of carbamazepine in surface freshwaters: Laboratory measures and modeling. Environ. Sci. Technol., 2012; 46: 8164-8173.

De Laurentiis, E., Prasse, C., Ternes, T.A., Minella, M., Maurino, V., Minero, C., Sarakha, M., Brigante M., Vione D., Assessing the photochemical transformation pathways of acetaminophen relevant to surface waters: Transformation kinetics, intermediates, and modelling. Water Res. 2014; 53: 235-248.

Fent K.; Zenker A.; Rapp M.; Widespread occurrence of estrogenic UV-filters in aquatic ecosystems in Switzerland; Environ. Pollution, 2010; 158: 1817–1824

Goksoyr A.; Tollefsen K.E.; Grung M.; Loken K.; Lie E.; Zenker A. Balsa raft crossing the Pacific finds low contaminant levels; Environ. Sci. Technol. 2009; 43:4783–90

Hanson K.M.; Gratton E.; Bardeen C.J.; Sunscreen enhancement of UV-induced reactive oxygen species in the skin; Free Rad. Biol. Med. 2006; 41: 1205–1212

Hauri, U.; Luetolf, B.; Schlegel, U.; Hohl, C. Determination of photodegradation of UV filters in sunscreens by HPLC/DAD and HPLC/MS. Mitteil. Lebensmitteil. Hyg. 2004; 95: 147-161

Janjua N.R.; Kongshoj B.; Andersson A.M; Wulf H.C.; Sunscreens in human plasma and urine after repeated wholebody topical application; J. Eur. Acad. Dermatol. Venereol. 2008; 22: 456–461

Kameda Y.; Kimura K.; Miyazaki M.; Occurrence and profiles of organic sunblocking agents in surface waters and sediments in Japanese rivers and lakes; Environ. Pollution 2011; 159, 1570–76

Kouloumbos V.N.; Tsipi D.F.; Hiskia A.E.; Nikolic D.; Van Breemen R.B.; Identification of photocatalytic degradation products of diazinon in TiO_2 aqueous suspensions using GC/MS/MS and LC/MS with quadrupole time-of-flight mass spectrometry; J. Am. Soc. Mass Spectrom. 2003; 14 (8): 803-817

Konstantinou I.K.; Sakellarides T.M.; Sakkas V.A.; Albanis T.A; Photocatalytic degradation of selected s-triazine herbicides and organophosphorus insecticides over aqueous TiO_2 suspensions; Environ. Sci. Technol., 2001; 35: 398-405

Kupper T; Plagellat C.; Brändli R.C.; de Alencastro L.F.; Grandjean D; Tarradellas J.; Fate and removal of polycyclic musks, UV filters and biocides during wastewater treatment; Water Res. 2006; 40:2603–2612

Li W.; Ma Y.; Guo C.; Hu W.; Liu K.; Wang Y.; Zhu T.; Occurrence and behavior of four of the most used sunscreen UV filters in a wastewater reclamation plant; Water Res. 2007; 41, 3506 –12

Magi E; Scapolla C.; Di Carro M.; Rivaro P.; Nguyen K.T.N; Emerging pollutants in aquatic environments: monitoring of UV filters in urban wastewater treatment plants; Anal. Methods, 2013; 5, 428-433.

Maddigapu P.R., Minella M., Vione D., Maurino V., Minero C. Modeling phototransformation reactions in surface water bodies: 2,4-Dichloro-6-nitrophenol as a case study. Environ. Sci. Technol., 2011; 45: 209-214.

Marchetti G., Minella M., Maurino V., Minero C., Vione D. Photochemical transformation of atrazine and formation of photointermediates under conditions relevant to sunlit surface waters: Laboratory measures and modelling. Wat. Res., 2013; 47: 6211-6222.

Marchisio A., Minella M., Maurino V., Minero C., Vione D., Photogeneration of reactive transient species upon irradiation of natural water samples: Formation quantum yields in different spectral intervals, and implications for the photochemistry of surface waters. Water Res. 2015, 73: 145-156.

Poiger T.; Buser H.R.; Balmer M.E.; Bergqvist P.A.; Müller M.D.; Occurrence of UV filter compounds from sunscreens in surface waters: regional mass balance in two Swiss lakes; Chemosphere 2004; 55:951–963

Rodil R.; Moeder M. Development of a method for the determination of UV filters in water samples using stir bar sorptive extraction and thermal desorption–gas chromatography–mass spectrometry; J. Chromat. A 2008; 1179:81–8

Rodil R.; Moeder,M; Altenburger R.; Schmitt-Jansen M.; Photostability and phytotoxicity of selected sunscreen agents and their degradation mixtures in water; Anal. Bioanal. Chem. 2009; 395:1513–1524

Ruggeri G.; Ghigo G.; Maurino V.; Minero C.; Vione D. Photochemical transformation of ibuprofen into harmful 4-isobutylacetophenone: Pathways, kinetics, and significance for surface waters. Water Res. 2014; 47: 6109-6121

Schlumpf M.; Cotton B.; Conscience M.; Haller V.; Steinmann B.; Lichtensteiger W.; In vitro and in vivo estrogenicity of UV screens; Environ. Health Perspect. 2001; 109 (3): 239-244

Tunkel J., Mayo K., Austin C., Hickerson A., Howard P., Practical considerations on the use of predictive models for regulatory purposes. Environ. Sci. Technol. 2005; 39 : 2188-2199.

Turro N.J., Ramamurthy V., Cherry W., Farneth W. The effect of wavelength on organic photoreactions in solution. Reactions from upper excited states. Chemical Rev. 1978; 78, 125-145.

Vione D, Maddigapu PR, De Laurentiis E, Minella M, Pazzi M, Maurino V, Minero C, Kouras S, Richard C. Modelling the photochemical fate of ibuprofen in surface waters. Wat Res 2011;45:6725-36.

Vione D., Minella M., Maurino V., Minero C. Indirect photochemistry in sunlit surface waters: Photoinduced production of reactive transient species. Chem.: A European J. 2014; 20: 10590-10606.

Figure captions

Fig. 1. Absorption spectrum (molar absorption coefficient $\varepsilon_{EHMC}(\lambda)$) of EHMC. Emission spectrum (spectral photon flux density p°(λ)) of the TL 01 RS lamp.

Fig. 2. (a) Modeled half-life time of EHMC (units of SSD = summer sunny days equivalent to 15 July at 45°N latitude) as a function of water depth and DOC. Other water conditions: 0.1 mM nitrate, 1 µM nitrite, 1 mM bicarbonate, 10 µM carbonate.
(b) Modeled time trends of EHMC and MOBA (SSD units) for the following water conditions: 5 m depth, 5 mg C L^{-1} DOC, 0.1 mM nitrate, 1 µM nitrite, 1 mM bicarbonate, 10 µM carbonate. For plot readability issues, the MOBA concentration was multiplied by 10. $MOBA_1$: k_{MOBA} = 0.01 SSD^{-1} ($k°_{MOBA}$); $MOBA_2$: k_{MOBA} = 2 SSD^{-1}; $MOBA_3$: k_{MOBA} = 6.6 SSD^{-1} (k'_{MOBA}).

Fig. 3. EHMC degradation under UVA or UVB lamp.

Fig. 4. Transformation products formed from EHMC over time under direct photolysis. The figure on the top shows the transformation products (TPs) formed under UVB, while in the bottom figure, the TPs formed under UVA are shown.

Fig. 5. EHMC degradation and transformation products formation profile over time in the presence of TiO_2. The top two figures show the most abundant TPs, while in the bottom one the less abundant TPs are shown.

Fig. 6. Proposed photoinduced transformation pathways followed by EHMC

Fig.7. Acute toxicity of EHMC as a function of irradiation time in the presence of TiO_2

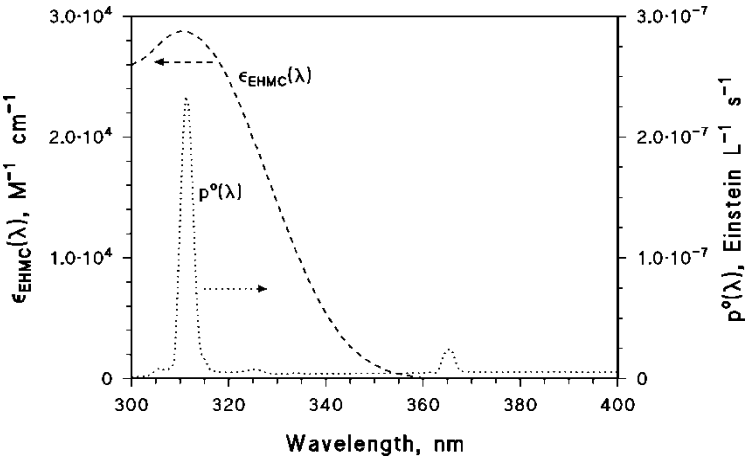
3.0·10⁴
2.0·10⁴
1.0·10⁴
0
3.0·10⁻⁷
2.0·10⁻⁷
1.0·10⁻⁷
0
300
320
340
360
380
400
Wavelength, nm
ε_EHMC(λ), M⁻¹ cm⁻¹
p°(λ), Einstein L⁻¹ s⁻¹
ε_EHMC(λ)
p°(λ)

Figure 1.

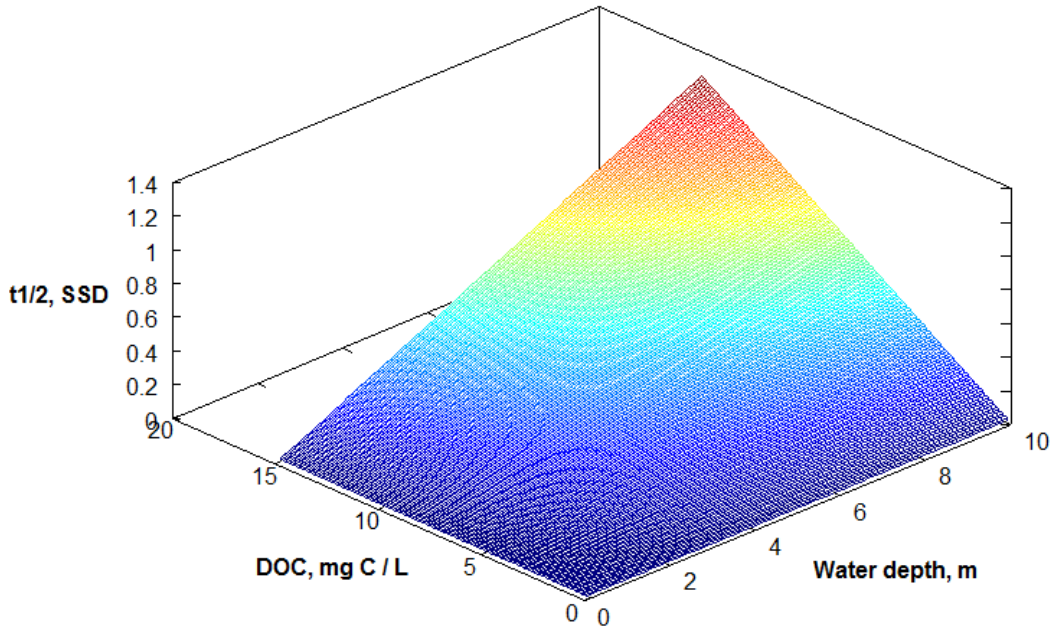
t1/2, SSD
1.4
1.2
1
0.8
0.6
0.4
0.2
0
20
15
10
5
0
DOC, mg C / L
0
2
4
6
8
10
Water depth, m

(a)

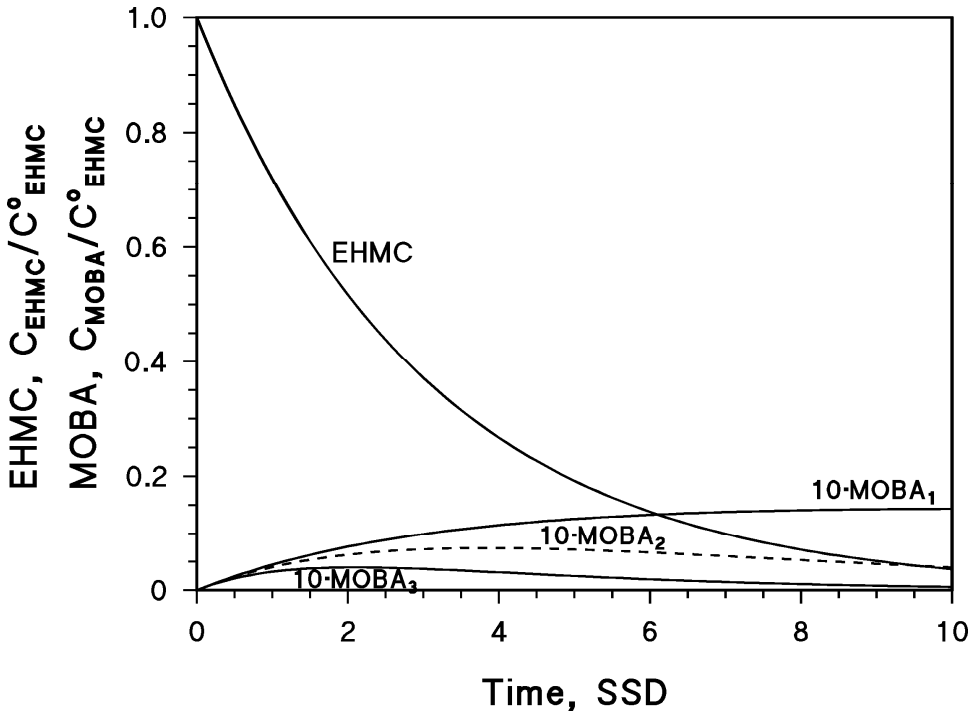
EHMC, C_{EHMC}/C^{o}_{EHMC}
MOBA, C_{MOBA}/C^{o}_{EHMC}
1.0
0.8
0.6
0.4
0.2
0
EHMC
10-MOBA$_1$
10-MOBA$_2$
10-MOBA$_3$
0
2
4
6
8
10
Time, SSD

(b)

Figure 2.

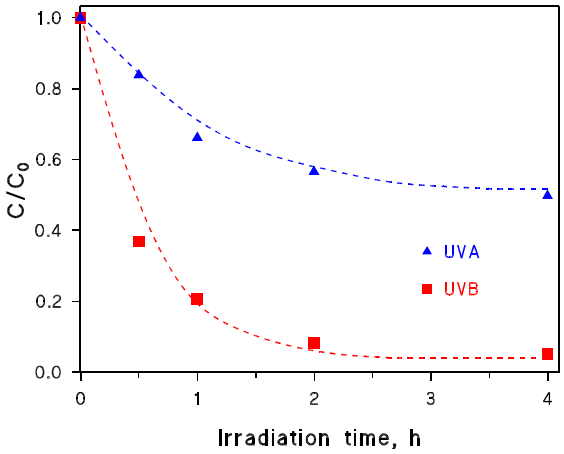

Figure 3.

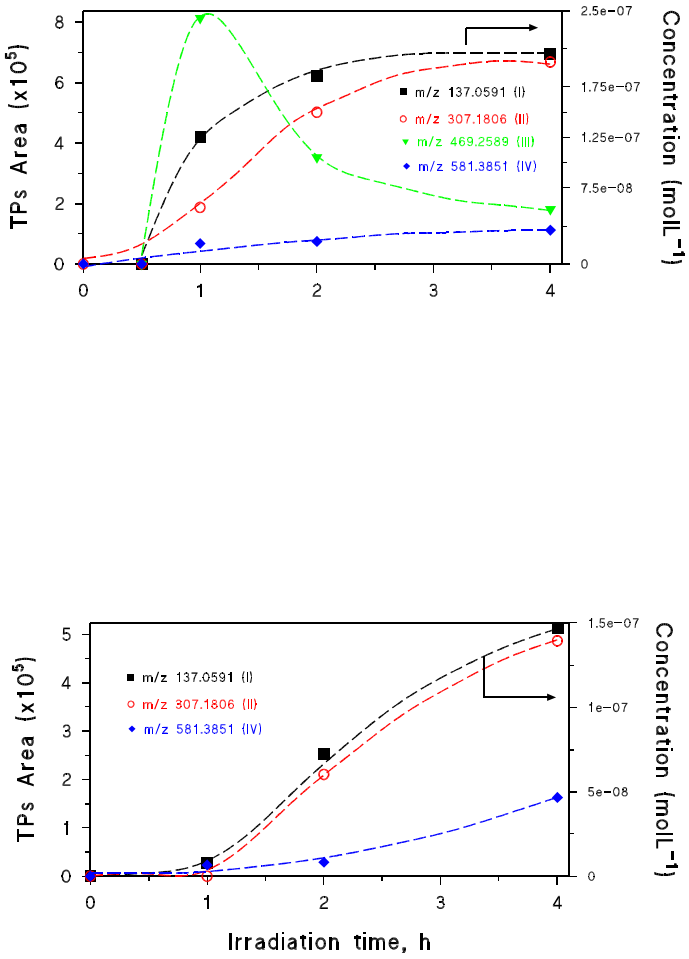
TPs Area (x10^5)
Concentration (molL^{-1})
m/z 137.0591 (I)
m/z 307.1806 (II)
m/z 469.2589 (III)
m/z 581.3851 (IV)
Irradiation time, h

Figure 4.

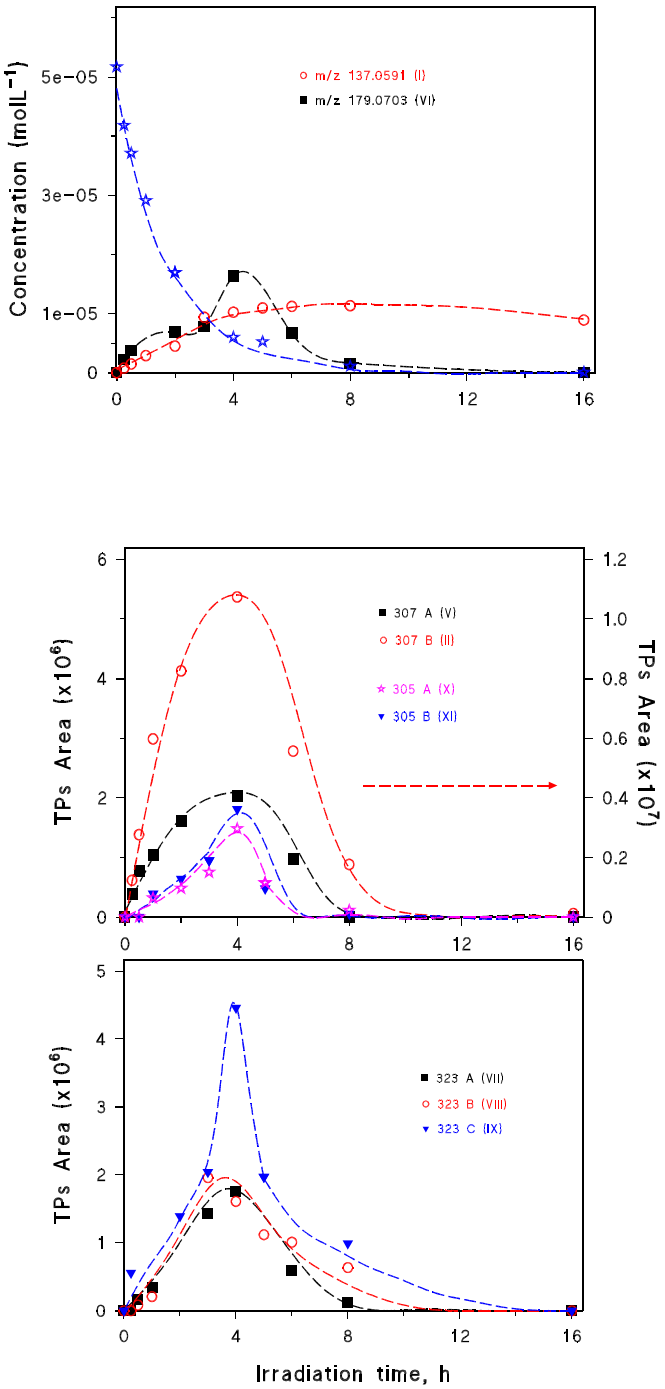
Concentration (molL^{-1})
5e−05
3e−05
1e−05
0
m/z 137.0591 (I)
m/z 179.0703 (VI)
0
4
8
12
16
TPs Area (x10^6)
TPs Area (x10^7)
307 A (V)
307 B (III)
305 A (X)
305 B (XI)
323 A (VII)
323 B (VIII)
323 C (IX)
Irradiation time, h

Figure 5.

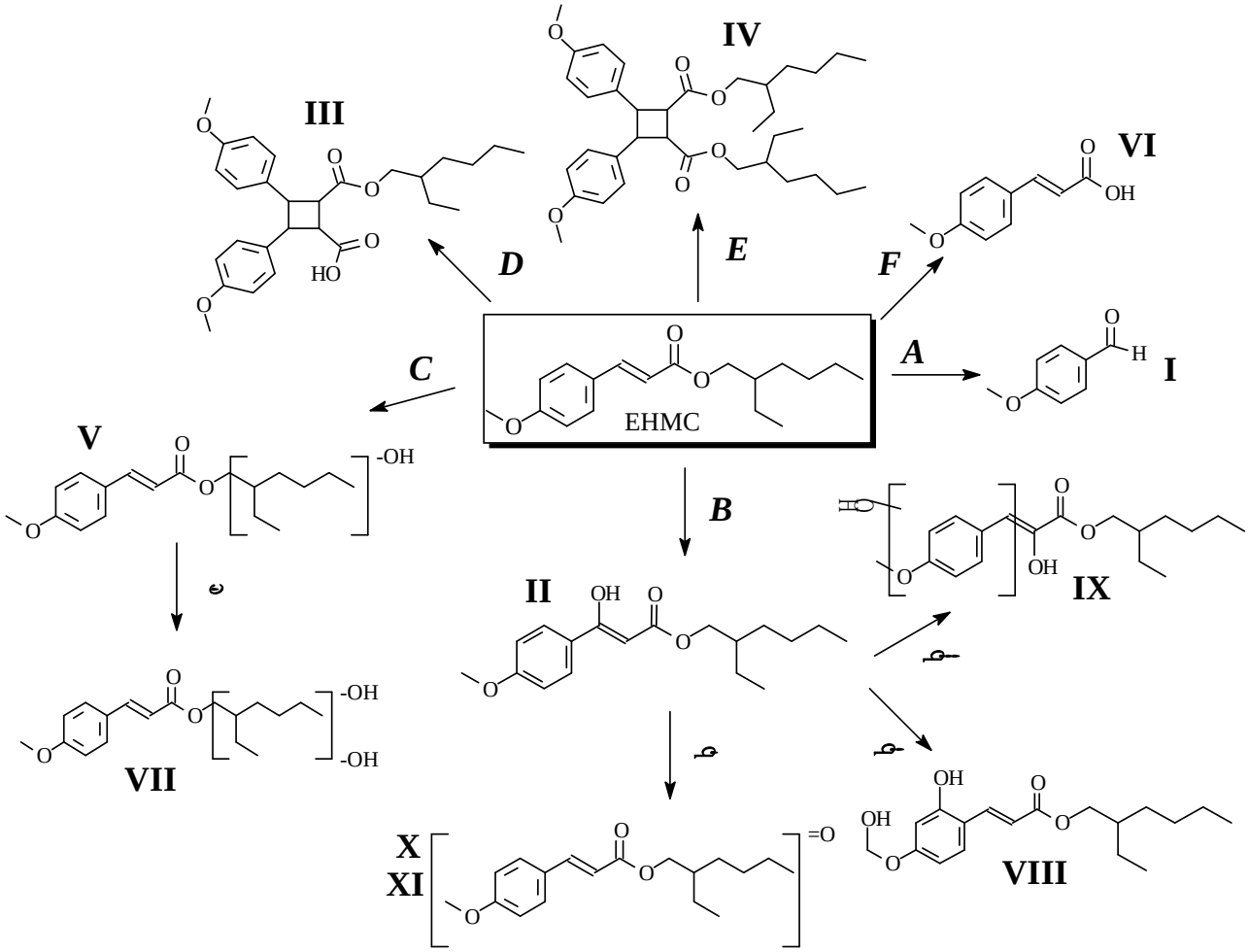

Figure 6.

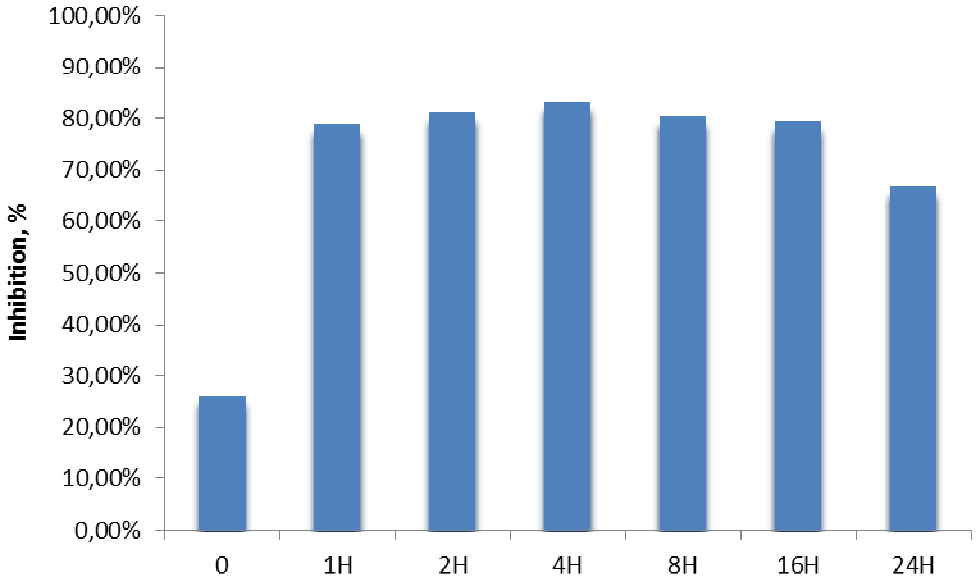
100,00%
90,00%
80,00%
70,00%
60,00%
50,00%
40,00%
30,00%
20,00%
10,00%
0,00%
Inhibition, %
0
1H
2H
4H
8H
16H
24H

Figure 7.

Table 1.Transformation products formed during direct photolysis or heterogeneous photocatalysis

$[M+H]^+$ and empirical formula	Number	Isomer	Δmmu	t_R (min)
137.0591 ($C_8H_9O_2$)	**I**	-	- 0.656	17.3
307.180 ($C_{18}H_{27}O_4$)	**II**	**307 B**	-0.954	32.1
307.1806 ($C_{18}H_{27}O_4$)	**V**	**307 A**	-0.954	25.7
469.2589 ($C_{28}H_{37}O_6$)	**III**	-	0.935	31.9
581.3851 ($C_{36}H_{53}O_6$)	**IV**	-	1.404	40.9
179.0703 ($C_{10}H_{11}O_3$)	**VI**	-	-0.489	35.9
323.1850 ($C_{18}H_{27}O_5$)	**VII**	**323 A**	-0.270	20.4
323.1850 ($C_{18}H_{27}O_5$)	**VIII**	**323 B**	-0.270	24.4
323.1850 ($C_{18}H_{27}O_5$)	**IX**	**323 C**	-0.270	29.6
305.1732 ($C_{18}H_{25}O_4$)	**X**	**305 A**	-1.546	27.9
305.1732 ($C_{18}H_{25}O_4$)	**XI**	**305 B**	-1.546	29.6